THE JOURNAL OF PHYSICAL CHEMISTRY A

Article

pubs.acs.org/JPCA

Thermal Effects Associated with the Raman Spectroscopy of WO_3 Gas-Sensor Materials

Raul F. Garcia-Sanchez,[†] Tariq Ahmido,[‡] Daniel Casimir,[†] Shankar Baliga,[§] and Prabhakar Misra*,[†]

[†]Department of Physics and Astronomy, Howard University, 2355 Sixth Street NW, Washington, DC 20059, United States

[‡]Aberdeen Proving Ground, 5158 Blackhawk Road, Aberdeen, Maryland 21010, United States

[§]General Monitors, 26776 Simpatica Circle, Lake Forest, California 92630, United States

Supporting Information

ABSTRACT: Metal oxides are suitable for detecting, through conductive measurements, a variety of reducing and oxidizing gases in environmental and sensing applications. Metal-oxide gas sensors can be developed with the goal of sensing gases under specific conditions and, as a whole, are heavily dependent on the manufacturing process. Tungsten oxide (WO_3) is a promising metal-oxide material for gas-sensing applications. The purpose of this paper is to determine the existence of a correlation between thermal effects and the changes in the Raman spectra for multiple WO_3 structures. We have obtained results utilizing Raman spectroscopy for three different structures of WO_3 (monoclinic WO_3 on Si substrate, nanopowder, and nanowires) that have been subjected to temperatures in the range of 30−160 °C. The major vibrational modes of the WO_3:Si and the nanopowder samples, located at ∼807, ∼716, and ∼271 cm^{-1}, correspond to the stretching of O−W−O bonds, the stretching of W−O, and the bending of O−W−O, respectively; these are consistent with a monoclinic WO_3 structure. However in the nanowires sample only asymmetric stretching of the W−O bonds occurs, resulting in a 750 cm^{-1} band, and the bending of the O−W−O mode (271 cm^{-1}) is a stretching mode (239 cm^{-1}) instead, suggesting the nanowires are not strictly monoclinic. The most notable effect of increasing the temperature of the samples is the appearance of the bending mode of W−OH bonds in the approximate range of 1550−1150 cm^{-1}, which is related to O−H bonding caused by humidity effects. In addition, features such as those at 750 cm^{-1} for nanowires and at 492 and 670 cm^{-1} for WO_3:Si disappear as the temperature increases. A deeper understanding of the effect that temperature has on the Raman spectral characteristics of a metal oxide such as WO_3 has helped to extend our knowledge regarding the behavior of metal oxide−gas interactions for sensing applications. This, in turn, will help to develop theoretical models for the identification of specific metal oxide−gas relationships.

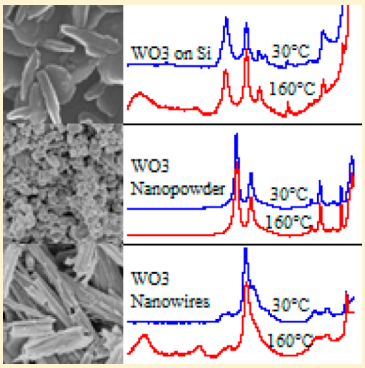

INTRODUCTION

Metal oxides gas sensors (MOGS) are suitable for detecting, through conductive measurements, a variety of reducing and oxidizing gases in environmental and sensing applications.[1−6] Some of their advantages include low cost, easy production, large number of detectable gases, simplicity of use, and compact size.[7] MOGS have been extensively used in the detection of a wide variety of greenhouse gases such as NO, N_2O, NO_2, CO, CO_2, SO_2, H_2S, NH_3, CH_4, and O_3.[8,9] The study of these gases is important not only for greenhouse effects but also for environmental contamination as they can be toxic on continuous exposure. Additionally, metal oxides have been shown to react with various hydrocarbons and alcohols.[1,2]

An n-type semiconductor contains an excess of free electrons, and, upon exposure to a reducing gas, an increase in conductivity occurs; the opposite is true for oxidizing gases.[3] WO_3 is an n-type semiconductor material with operational temperatures between 200 and 500 °C;[4] the sensor signal decreases drastically in the range from 150 to 300 °C.[5] WO_3 sensors are the most-used metal oxide gas sensors for the detection of NO_x.[6] WO_3 sensors are capable of measuring NO_x accurately in the 10 ppb range and operate at the lower threshold of operating temperatures (200−300 °C) usually associated with metal oxide gas sensors (200−500 °C). NO_x is found in smog and energetic materials; the detection of these radicals could be used for environmental monitoring. The detection of early smog formation and concentration can be determined through measuring NO. NO_2 is extremely toxic, and inhaling it can lead to respiratory problems. Studies have shown that high concentrations of NO_2 and SO_2 can lead to respiratory disease.[10] WO_3 films very sensitive to NO and NO_2 gases have been produced[11,12] that can discriminate NO/NO_2 from H_2 and CO. Studies have also been done on the effects of grain size on the response of WO_3 sensors.[13,14]

Investigations on the effects of gas exposure on a WO_3 powder's Raman features have been also been performed.[15,16] In these studies, the WO_3 powder was submitted to a change in atmosphere, and the Raman spectra undergo changes based on

Special Issue: Terry A. Miller Festschrift

Received: August 19, 2013
Revised: October 1, 2013
Published: October 2, 2013

   dx.doi.org/10.1021/jp408303p | J. Phys. Chem. A 2013, 117, 13825−13831

whether the atmosphere is reducing or oxidizing. The effect of CH_4 (a reducing gas) exposure to the WO_3 powder is the appearance of the 1300 and 1600 cm^{-1} bands in the Raman spectrum. As the CH_4 exposure continued, these bands become larger than the stretching mode (600−900 cm^{-1}). The intensity of the entire Raman spectrum increases, and the high-frequency bands disappear when the atmosphere is switched to 1000 ppm NO_2/N_2 (oxidizing gas). This suggests that the type of gas, the length of exposure, and other parameters can affect the Raman spectra of the WO_3 samples.

Raman spectroscopy[17] has been employed to investigate the correlation between thermal effects and the changes in the MOGS material's Raman spectra. Experiments involving Raman spectroscopy have explored gas-sensing applications.[18,19] Raman spectroscopy, coupled with DC resistance measurements, was used to investigate the H_2S-sensing capabilities of a SnO_2-based gas sensor.[18] Only recently studies on gas sensors using Raman spectroscopy in real-time conditions were performed.[20,21] Work was also done on an approach that applies multiple complementary methods (i.e., FT-IR and Raman, etc.) at the same time under conditions close to actual working conditions, which resulted in the discrimination of different reactions.[7,17] Temperature plays an important role in the adsorption behavior of metal oxide sensors and the associated Raman signatures of these samples.[22−26] It is well established that the signal from the sensor, under exposure for a target gas, increases until reaching a particular optimal operational temperature, and then the signal decreases with increasing temperature past that point, which yields a bell-shaped curve of the plot of signal versus temperature.[27] As a result, determining the optimal operating temperature for the MOGS samples is a critical parameter for the effective detection of specific target gases.

The chemisorption of oxygen is the main element in the change in conductance that occurs in metal-oxide gas sensors; adsorption and electron transfer occur via the chemisorption of oxygen, which occurs when the oxygen species occupy the lattice sites of the metal oxide at the surface.[28] Additionally, the oxygen species present in the environment, the charge of the oxygen species adsorbed by the sensor, and molecular adsorption are temperature-dependent.[29] For temperatures (T) < 150 °C, molecular oxygen (O_2^-) is present, while for T > 150 °C we have atomic oxygen (O^- at T = 150 − 300 °C; O^{2-} at T > 300 °C). The presence of ozone, which decays into molecular oxygen, can cause the oxygen vacancies in the sensor lattice to fill up,[30] increasing instead of decreasing sensor conductivity. Thus, attention must be paid to situations where ozone can affect the measurements. Finally, the oxidation reaction (i.e., adsorption, chemisorption) is an activated process, and its rate is affected by temperature. Studying this, and other effects, will lead to a wide variety of metal-oxide samples; the patterns related to the structure and Raman spectra of these samples can help to understand the reason for their sensing capabilities toward certain gases (e.g., NO_x, SO_2, etc.).

EXPERIMENTAL PROCEDURES

Three tungsten oxide (WO_3) samples were used for this study:

(1) General Monitors monoclinic WO_3 on silicon substrate (WO_3:Si). The silicon substrate has a drop-coated and furnace-fired dot of WO_3. The WO_3 is in the shape of platelets, and the film is porous. The WO_3 is about 2.5 mm in diameter and 4 μm thick.

(2) Sigma-Aldrich (#550086) WO_3 nanopowder. This yellow-greenish powder had a particle size of <100 nm (determined by transmission electron microscopy) and a density of 7.16 g/mL at 25 °C.

(3) Sigma-Aldrich (#774537) WO_3 nanowires. This white powder-like sample of diameter ∼50 nm and length of 10 μm had a density of 7.16 g/mL at 25 °C.

Figure 1 shows the high-resolution scanning electron microscope (SEM) images of our three samples at different scales. The WO_3:Si SEM image was provided by the manufacturer, and a JEOL JSM-6360 LV SEM was used for the nanopowder and nanowire samples.

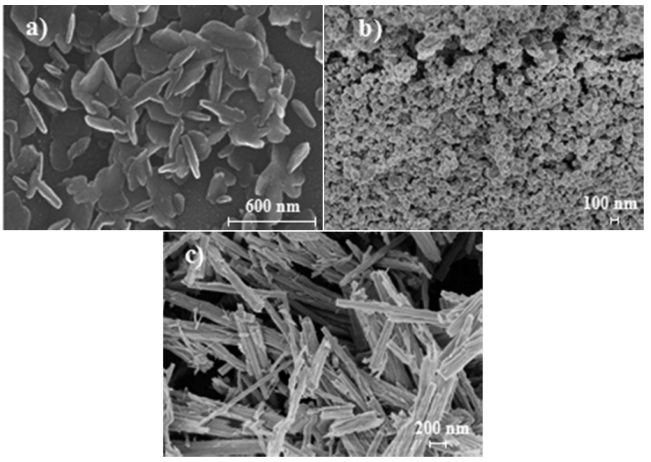

Figure 1. SEM images of (a) WO_3:Si, (b) WO_3 nanopowder, and (c) WO_3 nanowires, at 600, 100, and 200 nm scales, respectively.

The data for the Raman study of these samples were taken using a Thermo Scientific DXR Smart Raman spectrometer. The light source used in this spectrometer is a continuous wave (CW) laser that emits at 780 ± 0.2 nm with the laser beam quality of $M^2 \leq 1.5$.[31] Figure 2 shows the Raman instrument experimental setup.

The laser beam, the diameter of which is 3.5 mm, is focused on the samples using an objective lens. The smallest footprint size of the focused beam is estimated to be less than 10 μm. The laser power is adjustable and ranges from 0.1 mW to 24 mW in increments of 0.1 mW. In addition to the adjustment of power, the samples were also placed on a three-dimensional translation stage (x, y, and z), where z represents the laser propagation axis. The translation through the z direction permits additional control over the laser irradiance on the sample.

In this experiment, the samples were placed at the laser focus point and exposed to 14 mW of laser power. The collection time per exposure of the sample to the laser beam was 10 s, averaged over 12 sample exposures, for each of the three samples. With a spot size of approximately 10 μm in diameter, the power density was 17.834 kW/cm^2.

The Raman signal was collected using the objective lens mentioned above and an additional collection lens (see Figure 2). The collected signals were focused at the input slit of the spectrograph and imaged at the imaging plane of the input slit. At the output, a 2048 pixel one-dimensional array charge-coupled device (CCD) detector was placed at the imaging plan

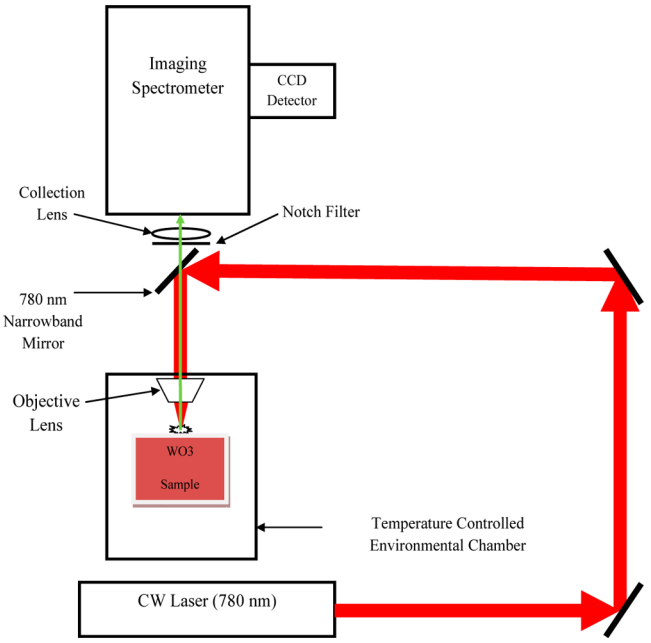

Figure 2. Schematic of Raman spectrometer experimental setup collection.

of the spectrometer. The groove density of the diffraction grating was 400 grooves/mm, and the spectrometer was able to resolve features up to 3 cm^{-1}. With this diffraction grating, with the given spectrometer *f*-number and CCD detector size, the spectrometer was able to capture a full range of spectra from 50 cm^{-1} to the upper cutoff of 3000 cm^{-1}.

The spectrometer must be calibrated and aligned before preparing the sample and taking data. In order to complete these two procedures, a software-controlled DXR Smart Raman accessory was used for alignment and calibration. To verify that the alignment and calibration was accurate, a Si substrate film similar to the one used for the WO_3:Si sample was placed to ensure that the Si Raman peak is located at 520 cm^{-1}.[23,32]

All three samples were tested at room temperature inside a temperature-controlled chamber located inside the spectrometer chamber. The model H4 200 cell from Ventacon Ltd. allowed us to heat solid, liquid, or semisolid samples to elevated temperatures (up to 200 °C) within the DXR Smart Raman instrument chamber. The cavity containing the sample can be evacuated or filled with gas. The cell uses a Series D Power Supply that provides a stabilized DC voltage of 24 V in order to control the heating process and to monitor the temperature of the hot cell; the temperature sensing and control are achieved using a calibrated differential proportional controller.

The spectral data analysis carried out was in the temperature range from 30 to 160 °C. The temperature was controlled and could be increased in increments of 0.1 °C. During the data collection, the temperature was increased by 10 °C each time. In order to verify that the data obtained were reproducible, the data were collected on different days under similar environmental conditions. The experimental values discussed are summarized in Table 1.

RESULTS AND DISCUSSION

The WO_3 monoclinic lattice structure is composed of WO_6 octahedra, is stable at room temperature, and has two temperature-related transitions, namely, the monoclinic-orthorhombic and the orthorhombic-hexagonal.[25] However, within the temperature range studied, these WO_3 transitions did not occur. The major vibrational modes for the WO_3 lattice are the stretching (ν), the bending (δ), and the out-of-plane wagging (γ) modes.[33]

Figure 3 shows the change in the Raman spectra of all three samples as the temperature increases. The temperature goes up 10 °C for every Raman spectra shift downward, going from 30 to 160 °C for all samples. Tables 2, 3, and 4 show the Raman bands associated with each sample at the minimum and maximum experimental temperatures and their corresponding peak assignments.

For the WO_3:Si sample, we observe that the peak at 1550 cm^{-1} starts showing up at 130 °C. The modes associated with this wavenumber correspond to the bending of O−H in the W−OH bond formed by the exposure of the WO_3 lattice to humidity, introducing OH/H_2O bonds into it. This suggests that, as the temperature increases, the humidity-affected WO_3 monoclinic lattice's W−OH bonds are pulling more strongly than the W═O bonds that occur naturally in the lattice. Additionally, the 670 and 492 cm^{-1} bands disappear as the temperature increases, specifically, from 130 °C onward. In the case of the peak at 492 cm^{-1}, we see that this feature shares a broad band with that at 519 cm^{-1} (which also corresponds to the O-lattice vibrational mode). However once 130 °C is reached, the 516 cm^{-1} peak becomes far clearer than it is at lower temperatures; this suggests a combination of the O-lattice vibrations as the temperature increases. The WO_3:Si sample also exhibits the 808, 714, and 270 cm^{-1} Raman modes, confirming that it is indeed monoclinic.

For the nanopowder, the temperature variations do not seem to change the overall Raman spectral bands outside the low-frequency phonon temperature change marker modes. This suggests that no changes or deformations to the structure of the sample occur in the temperature range studied. Evidence of this has been seen in the Raman spectroscopy of LiB_3O_5 and $Li_2B_4O_7$ under both heating and melting conditions, there being no deformations occurring at certain temperature steps.[34] As the nanopowder, unlike the other two samples, does not exhibit W−OH or O−H bonds in its structure with increasing temperature, it is plausible that the lack of change is related to the aforementioned bond absence.

A behavior similar to that of the WO_3:Si sample occurs in the nanowire sample, in which the ∼670 cm^{-1} peak also disappears with increasing temperature. In addition, the nanowire feature at 758 cm^{-1} begins to flatten out as the temperature increases

Table 1. Parameter Values for Experimental Setup

power (mW)	exposure time (s)	laser spot diameter (μm)	sample distance to objective lens (cm)	temperature range (°C)	temperature step (°C)	power density (kW/cm^2)
14	120	10	0.8 (nanowires) 1.0 (nanopowder) 1.3 (WO_3:Si)	30−160	10	17.834

dx.doi.org/10.1021/jp408303p | J. Phys. Chem. A 2013, 117, 13825−13831

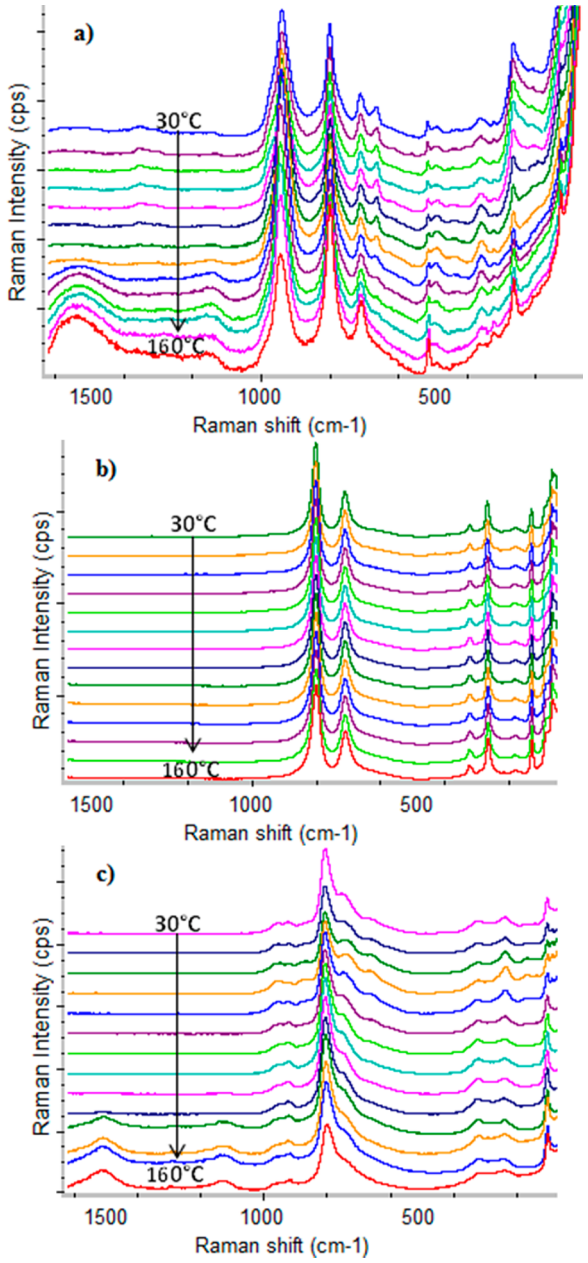

Figure 3. Change in Raman spectra with increasing temperature for (a) monoclinic WO_3:Si, (b) WO_3 nanopowder, and (c) WO_3 nanowires in the range of 30−160 °C.

as well. The appearance of the ∼1140 cm^{-1} band as the temperature increases is due to the bending of the W−OH bonds.[38]

Figure 4 shows the Raman spectra for all three samples at (a) 30 °C and (b) 160 °C. The differences between the Raman spectra are as follows:

(1) A broad Raman band appears in the 1550 cm^{-1} range corresponding to W−OH bonding for the WO_3:Si and the nanowires.
(2) The nanopowder does not exhibit a stretching mode around 950 cm^{-1}.
(3) While the WO_3:Si sample and the nanopowder exhibit the typical W−O stretching at ∼714 cm^{-1}, the nanowires only exhibit asymmetric stretching of the W−O bonds, resulting in a larger Raman shift of the 750 cm^{-1} feature.
(4) The out-of-plane wagging γ(O−W−O) at 670 cm^{-1} is not present for the nanopowder.
(5) The peak at 270 cm^{-1} associated with the bending of the dangling oxygen, δ(O−W−O), in the monoclinic structure is not present in the nanowires. Instead, two peaks, at 328 and 239 cm^{-1}, corresponding to δ(O−W−O) and ν(O−W−O), respectively, are present.
(6) While the nanopowder sample remains fairly constant (aside from the Raman shifts related to the temperature and the spectral resolution of the instrument) as the temperature increases, the WO_3:Si and the nanowires have Raman features that appear (1550 cm^{-1}) and disappear (670 cm^{-1}) as the temperature increases.

The major vibrational modes of the WO_3:Si sample and the nanopowder, located at ∼807, ∼716, and ∼271 cm^{-1}, corresponding to the stretching of O−W−O, the stretching of W−O, and the bending of O−W−O, respectively, are consistent with a monoclinic WO_3 structure.[22] All three modes are present in the WO_3:Si sample and the nanopowder, suggesting a proper monoclinic structure. However, the nanowires exhibit a stretching of O−W−O in place of the bending, resulting in a 240 cm^{-1} peak; additionally, only asymmetrical stretching related to general metal-oxide bonding ν_a(M−O), resulting in a 750 cm^{-1} band, is observed, instead of the monoclinic 714 cm^{-1} feature.

A peak forms in the ∼1550 cm^{-1} region for both the WO_3:Si and the WO_3 nanowires samples as the temperature increases. Although this feature is not as distinct for the WO_3 nanopowder, we were able to reproduce a similar behavior in the ∼1460 cm^{-1} region by exposing three WO_3 nanopowder samples to two different humidity conditions (Raman spectral data on the humid nanopowder can be found in the Supporting Information). Sample 1 (moist) was made by leaving 0.9 g of nanopowder in a ∼60% humidity environment for 5 days. Sample 2 (damp) was made by leaving 0.9 g of nanopowder in a ∼75% humidity environment for 5 days. Sample 3 (wet) was prepared by mixing 0.5 mL of water with 0.9 g of nanopowder.

The above humidity experiment suggests that the observed feature is due to the bonding of WO_3 with H_2O and is verified by multiple sources.[23,33,35,36] We have also reproduced this behavior by exposing the WO_3 nanopowder sample, which did not show this feature initially, to variable humidity; the Raman spectra for the different WO_3 nanopowder samples (with and without humidity and WO_3−H_2O) can be found in the Supporting Information. Additionally all samples have Raman bands below 200 cm^{-1}, which correspond to low-frequency phonon mode markers associated with temperature changes.[24,42]

CONCLUSIONS

We have studied the effect of temperature increases from 30 to 160 °C for three different WO_3 samples, namely, WO_3:Si, WO_3 nanopowder, and WO_3 nanowires. The temperature increase leads to an increase in the intensity of W−OH-related vibration modes, likely due to those bonds reacting more strongly to the temperature change than the normal W−O bonds related to the original lattice structure. In addition, we have seen that, for WO_3:Si and WO_3 nanopowder, the monoclinic vibrational modes remained fairly constant within the experimental temperature range, which suggests that no transitions occurred

Table 2. Summary of WO_3:Si Raman Bands

Raman band (cm^{-1}) sample temperature = 30 °C	Raman band (cm^{-1}) sample temperature = 160 °C	peak assignments
1537	1553	(a) δ OH in W–OH[35,36] (b) δ (OH–O)[23]
1361		ν OH, δ OH[37]
	1164	δ W–OH[38]
945	948	ν (O–W–O)[23] ν (W═O terminal)[23,36]
805	804	ν (O–W–O) (monoclinic phase)[22,39]
715	716	ν (W–O)[40]
670		γ (O–W–O)[35,36]
519	516	O-lattice[38,40]
492		O-lattice[38,40]
366	360	δ (O–W–O)[41]
326	326	δ (O–W–O)[26,40]
270	268	δ (O–W–O) in monoclinic structure[40]
131	131	low-frequency phonon temperature change marker[24,42]

Table 3. Summary of WO_3 Nanopowder Raman Bands

Raman band (cm^{-1}) sample temperature = 30 °C	Raman band (cm^{-1}) sample temperature = 160 °C	peak assignments
808	807	ν (O–W–O) (monoclinic phase)[22,39]
717	716	ν (W–O)[40]
436	438	WO_2W group bridged vibrations[39]
376	372	δ (O–W–O)[41]
328	328	δ (O–W–O)[26,40]
273	271	δ (O–W–O) in monoclinic structure[40]
221	220	W–W[43]
187	186	low-frequency phonon temperature change marker[24,42]
136	134	low-frequency phonon temperature change marker[24,42]
	88	low-frequency phonon temperature change marker[24,42]
71		low-frequency phonon temperature change marker[24,42]
63	68	low-frequency phonon temperature change marker[24,42]

Table 4. Summary of WO_3 Nanowires Raman Bands

Raman band (cm^{-1}) sample temperature = 30 °C	Raman band (cm^{-1}) sample temperature = 160 °C	peak assignments
	1523	(a) δ OH in W–OH[35,36] (b) δ (OH–O)[23]
	1145	δ W–OH[38]
954		ν (W═O terminal)[23,36]
930		ν_a (WO_2)[44,45]
	924	ν (W–O)[36]
812	807	ν (O–W–O) (monoclinic phase)[22,39]
758	749	ν_a (transition metal oxide bond)[46]
670		γ (O–W–O)[35,36]
328	321	δ (O–W–O)[26,40]
239	248	ν (O–W–O)[47]
145		low-frequency phonon temperature change marker[24,42]
108	106	low-frequency phonon temperature change marker[24,42]
93		low-frequency phonon temperature change marker[24,42]

in the WO_3 lattice structure. The γ(O–W–O) mode at 670 cm^{-1} disappears as the temperature increases for WO_3:Si and WO_3 nanowires samples. Such behavior suggests that, as the temperature increases, the angular molecular vibrations are dominated by the vibrations relating to the expansion and contraction of the bonds themselves (i.e., stretching and bending). For lower wavenumbers, the nonannealed samples—nanopowder and nanowires—exhibit different low-frequency phonons temperature change marker modes.

We will extend this work to include other parameters that can potentially affect the Raman spectrum of the materials, such as using a variety of reducing/oxidizing gas cycles and different concentrations and exposure times; these have been shown to affect the Raman spectra of metal oxide materials. Increasing the temperature range and carrying out thermal effect studies on wet WO_3 nanopowder samples would provide insight into the invariant spectral features found for this sample. This, in turn, would allow us to determine the effect that O–H- and W–OH-related bonds might have on the disappearance of

dx.doi.org/10.1021/jp408303p | J. Phys. Chem. A 2013, 117, 13825–13831

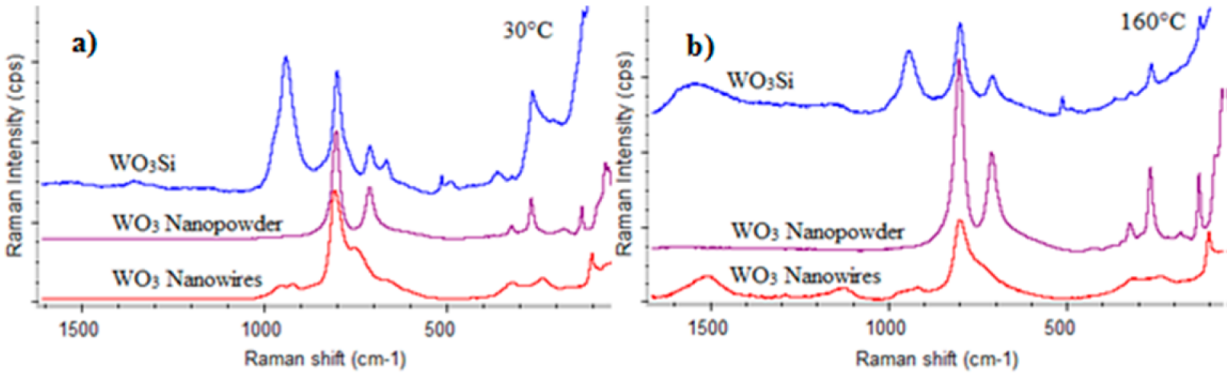

Figure 4. Raman spectra comparison for the three WO_3 samples at (a) 30 °C and (b) 160 °C.

some of the Raman features for both the WO_3:Si and the nanowires samples. Additionally, we can extend this work to include a comparison of polymorphs (triclinic, hexagonal, etc.) of the same material in a sensor and how the Raman features change when the polymorphs are compared with bulk samples of said materials, which can be done for a variety of metal oxide bulk samples. The manufacturing process that produces the entire sensor system can have effects on the material properties. Such manufacturing techniques can be used to increase/decrease the sensitivity to gases that are not of interest for the sensor application in mind.

■ ASSOCIATED CONTENT

Supporting Information

Raman spectra with peak assignments for three separate WO_3 nanopowder samples under (1) 60% humidity (moist sample), (2) 75% humidity (damp sample), and (3) mixed with H_2O (wet sample). This material is available free of charge via the Internet at http://pubs.acs.org.

■ AUTHOR INFORMATION

Corresponding Author

*E-mail: pmisra@howard.edu. Tel.: 202-806-6249.

Notes

The authors declare no competing financial interest.

■ ACKNOWLEDGMENTS

The authors would also like to thank Dr. Tongxin Wang and Dr. James Mitchell of the CREST Center for Nanomaterials, College of Engineering, Architecture and Computer Science, Howard University, for recording the SEM images of the WO_3 samples. Financial support from the NASA MIRS UNCF Special programs is gratefully acknowledged. The views expressed in this article are the views of the authors and do not reflect the official policy or position of the Department of the Army, the Department of Defense, or the U.S. Government. Use of trademarked name does not imply endorsement by the U.S. Army, but is intended only to assist in identification of a specific product.

■ REFERENCES

(1) Wang, Z.; Hu, X. Fabrication and electrochromic properties of spin-coated TiO_2 thin films from peroxo-polytitanic acid. *Thin Solid Films* **1999**, *352*, 62−65.

(2) Vaishanv, V. S.; Patel, P. D.; Patel, N. G. Indium tin oxide thin-film sensor for detection of Volatile Organic Compounds (VOCs). *Mater. Manuf. Process.* **2006**, *21*, 257−261.

(3) Jimenez-Cadena, G.; Riu, J.; Rius, F. X. Gas sensors based on nanostructured materials. *Analyst* **2007**, *132*, 1083−1099.

(4) Su, P. G.; Pan, T. T. Fabrication of a room-temperature NO_2 gas sensor based on WO_3 films and WO_3/MWCNT nanocomposite films by combining polyol process with metal organic decomposition method. *Mater. Chem. Phys.* **2011**, *125*, 351−357.

(5) Polleux, J.; Gurlo, A.; Barsan, N.; Weimar, U.; Antonietti, M.; Niederberger, M. Template-free synthesis and assembly of single-crystalline tungsten oxide nanowires and their gas sensing capabilities. *Angew. Chem., Int. Ed.* **2006**, *45*, 261−265.

(6) Fine, G. F.; Cavanagh, L. M.; Afonja, A.; Binions, R. Metal Oxide Semi-Conductor Gas Sensors in Environmental Monitoring. *Sensors* **2010**, *10*, 5469−5502.

(7) Barsan, N.; Weimar, U. Understanding the fundamental principles of metal oxide based gas sensors; the example of CO sensing with SnO_2 sensors in the presence of humidity. *J. Phys.: Condens. Matter* **2003**, *15*, R813.

(8) Wetchakun, K.; Samerjai, T.; Tamaekong, N.; Liewhiran, C.; Siriwong, C.; Kruefu, V.; Wisitsoraat, A.; Tuantranontb, A.; Phanichphanta, S. Semiconducting metal oxides as sensors for environmentally hazardous gases. *Sens. Actuators, B* **2011**, *160*, 580−591.

(9) Kanan, S. M.; El-Kadri, O. M; Abu-Yousef, I. A.; Kanan, M. C. Semiconducting Metal Oxide Based Sensors for Selective Gas Pollutant Detection. *Sensors* **2009**, *9*, 8158−8196.

(10) Ponka, A.; Virtanen, M. Chronic bronchitis, emphysema, and low-level air pollution in Helsinki, 1987−1989. *Environ. Res.* **1994**, *65*, 207−217.

(11) Akiyama, M.; Tamaki, J.; Miura, N.; Yamazoe, N. Tungsten oxide-based semiconductor sensor highly sensitive to NO and NO_2. *Chem. Lett.* **1991**, *20*, 1611−1614.

(12) Kida, T.; Nishiyama, A.; Yuasa, M.; Shimanoe, K.; Yamazoe, N. Highly sensitive NO_2 sensors using lamellar-structured WO_3 particles prepared by an acidification method. *Sens. Actuators, B* **2009**, *135*, 568−574.

(13) Tamaki, J.; Zhang, Z.; Fujimori, K.; Akiyama, M.; Harada, T.; Miura, N.; Yamazoe, N. Grain-size effects in tungsten oxide-based sensor for nitrogen oxides. *J. Electrochem. Soc.* **1994**, *141*, 2207−2210.

(14) Lee, D. S.; Han, S. D.; Huh, J. S.; Lee, D. D. Nitrogen oxides-sensing characteristics of WO_3-based Nanocrystalline thick film gas sensor. *Sens. Actuators, B* **1999**, *60*, 57−63.

(15) Boulova, M.; Gaskov, A.; Lucazeau, G. Tungsten oxide reactivity versus CH_4, CO and NO_2 molecules studied by Raman spectroscopy. *Sens. Actuators, B* **2001**, *81*, 99−106.

(16) Sergent, N.; Epifani, M.; Pagnier, T. In situ Raman spectroscopy study of NO_2 adsorption onto nanocrystalline tin(IV) oxide. *J. Raman Spectrosc.* **2006**, *37*, 1272−1277.

(17) Barsan, N.; Koziej, D.; Weimar, U. Metal oxide-based gas sensor research: How to? *Sens. Actuators, B* **2007**, *121*, 18−35.

(18) Pagnier, T.; Boulova, M.; Galerie, A.; Gaskov, A.; Lucazeau, G. In situ coupled Raman and impedance measurements of the reactivity

of Nanocrystalline SnO_2 versus H_2S. *J. Solid State Chem.* **1999**, *143*, 86−94.
(19) Itoh, T.; Toshiteru, M.; Atsuo, K. In situ surface-enhanced Raman scattering spectroelectrochemistry of oxygen species. *Faraday Discuss.* **2006**, *132*, 95−109.
(20) Sänze S.; Hess C. Metal Oxide-Based Gas Sensors VII, Operando Spectroscopic Study of the EtOH Gas Sensing Mechanism of In_2O_3. In *The 14th International Meeting on Chemical Sensors—IMCS 2012*, Nuremberg, Germany, May 20−23, 2012, Zintl Institute for Inorganic and Physical Chemistry, The Technical University Darmstadt: Darmstadt, Germany, 2012, pp 613−615; DOI 10.5162/IMCS2012/7.3.1.
(21) Sänze, S.; Gurlo, A.; Hess, C. Monitoring Gas Sensors at Work: Operando Raman-FTIR Study of Ethanol Detection by Indium Oxide. *Angew. Chem., Int. Ed.* **2013**, *52*, 3607−3610.
(22) Chan, S. S.; Wachs, I. E.; Murrell, L. L.; Dispenziere, N. C., Jr. Laser Raman Characterization of Tungsten Oxide Supported on Alumina: Influence of Calcination Temperatures. *J. Catal.* **1985**, *92*, 1−10.
(23) Santato, C.; Odziemkowski, M.; Ulmann, M.; Augustynski, J. Crystallographically Oriented Mesoporous WO_3 Films: Synthesis, Characterization, and Applications. *J. Am. Chem. Soc.* **2001**, *123*, 10639−10649.
(24) Salje, E.; Viswanathan, K. Physical Properties and Phase Transitions in WO_3. *Acta Crystallogr., Sect. A* **1975**, *31*, 356−359.
(25) Ramana, C. V.; Utsunomiya, S.; Ewing, R. C.; Julien, C. M.; Becker, U. Structural Stability and Phase Transitions in WO_3 thin films. *J. Phys. Chem. B* **2006**, *110*, 10430−10435.
(26) Rougier, A.; Portemer, F.; Quede, A.; Marssi, E. I. M. Characterization of pulsed laser deposited WO_3 thin films for electrochromic devices. *Appl. Surf. Sci.* **1999**, *153*, 1−9.
(27) Ahlers, S.; Muller, G.; Doll, T. A rate equation approach to the gas sensitivity of thin film metal oxide materials. *Sens. Actuators, B* **2005**, *107*, 587−599.
(28) Gopel, W.; Schierbaum, K. D. SnO_2 sensors: current status and future prospects. *Sens. Actuators, B* **1995**, *26*, 1−12.
(29) Bochenkov, V. E.; Sergeev, G. B. Sensitivity, Selectivity, and Stability of Gas-Sensitive Metal-Oxide Nanostructures. In *Metal Oxide Nanostructures and their Applications*; Umar, A., Hahn, Y.-B., Eds.; American Scientific Publishers: Valencia, CA, 2010; ISBN: 1-58883-176-0, Vol. *3*, pp 31−52.
(30) Zhao, Y. Design of Higher-k and More Stable Rare Earth Oxides as Gate Dielectrics for Advanced CMOS Devices. *Mater.* **2012**, *5*, 1413−1438.
(31) Thermo Scientific. DXR Smart Raman spectrometer product specification.
(32) From the Research Laboratory to the Process Line. In *Handbook of Raman Spectroscopy*, 1st ed.; Lewis, I. R., Edwards, H., Eds.; CRC Press: Boca Raton, FL, 2001; p 179.
(33) Cui H.-N. Preparation and Characterization of Optical Multilayered Coatings for Smart Windows Applications. *Doctoral Thesis*, University of Minho, Braga, Portugal, 2005.
(34) Voronko, Y. K.; Sobol, A. A.; Shukshin, V. E. Raman Spectroscopy Study of the Phase Transformatons of LiB_3O_5 and $Li_2B_4O_7$ during Heating and Melting. *Inorg. Mater.* **2013**, *49*, 923−929.
(35) Willis, H. A.; van der Maas, J. H.; Miller, R. G. J. *Laboratory Methods in Vibrational Spectroscopy*, 3rd ed.; John Wiley & Sons: New York, 1987.
(36) Pfeifer, J.; Guifang, C.; Tekula-Buxbaum, P.; Kiss, B. A.; Farkas-Jahnke, M.; Vadasdi, K. A reinvestigation of the preparation of tungsten oxide hydrate WO_3, $1/3H_2O$. *J. Solid State Chem.* **1995**, *119*, 90−97.
(37) Atanassor, G.; Thielsch, R.; Popor, D. Optical properties of TiO_2, Y_2O_3 and CeO_2 thin films deposited by electron beam evaporation. *Thin Solid Films* **1993**, *223*, 288−292.
(38) Wright, C. J. Inelastic neutron scattering spectra of the hydrogen tungsten bronze $H_{0.4}WO_3$. *J. Solid State Chem.* **1977**, *20*, 89−92.
(39) Keshavan, B.; Gowda, K. Dioxobridged complexes of molybdenum (IV) and tungsten (IV) with N-alkylphenothiazines and their interactions with L-cysteine and L-histidine. *J. Chem. Sci.* **2001**, *113*, 165−172.
(40) Daniel, M. F.; Desbat, B.; Lassegues, J. C.; Gerand, B.; Figlarz, M. Infrared and Raman study of WO_3 tungsten trioxides and WO_3, xH_2O tungsten trioxide hydrates. *J. Solid State Chem.* **1987**, *67*, 235−247.
(41) van der Vlies, A.-J. *Chemical Principles of the Sulfidation Reaction of Tungsten Oxides*. Dissertation Thesis, Swiss Federal Institute of Technology, Zurich, 2002.
(42) Collaboration: Authors and editors of the volumes III/17G-41D. *WO_3: phonon wavenumbers, Debye temperature*. Madelung, O., Rössler, U., Schulz, M., Eds.; *SpringerMaterials*, The Landolt—Börnstein Database.
(43) Lee, S.-H.; Cheong, H. M.; Tracy, C. E.; Mascarenhas, A.; Benson, D. K.; Deb, S. K. Raman spectroscopic studies of electrochromic a-WO_3. *Electrochim. Acta* **1999**, *44*, 3111−3115.
(44) Yoder, M. J. High temperature arc studies of infrared radiation from boron and tungsten oxides. *J. Quant. Spectrosc. Radiat. Transfer* **1974**, *14*, 1317−1328.
(45) Nagai, J. Optical and Chemical Properties of Electrochromic Oxide Films for Smart Windows. *Electrochim. Acta* **2001**, *46*, 2049−2053.
(46) Chuah, L. S.; Song, G.; Tang, G. Raman and SEM Characterization of Electrospun WO_3 Nanofibers. *Adv. in Optoelectron. Mater.* **2013**, *1*, 1−3.
(47) Regragui, M.; Addou, M.; Outzourhi, A.; Bernede, J. C.; El Idrissi, E.; Benseddik, E.; Kachouane, A. Preparation and characterization of pyrolytic spray deposited electrochromic tungsten trioxide films. *Thin Solid Films* **2000**, *358*, 40−45.